Aging of Iron (Hydr)oxides by Heat Treatment and Effects on Heavy Metal Binding

METTE A. SØRENSEN,*,†
MAIRAD M. STACKPOOLE,‡
ANATOLY I. FRENKEL,§
RAJENDRA K. BORDIA,‡
GREGORY V. KORSHIN,‖ AND
THOMAS H. CHRISTENSEN†

Department of Environmental Science and Engineering, Technical University of Denmark, Building 115, DK-2800 Kgs. Lyngby, Denmark, Materials Research Laboratory, University of Illinois at Urbana–Champaign, Urbana, Illinois 61801, Department of Material Science and Engineering and Department of Civil and Environmental Engineering, University of Washington, Seattle, Washington 98195

Amorphous iron (hydr)oxides are used to remove heavy metals from wastewater and in the treatment of air pollution control residues generated in waste incineration. In this study, iron oxides containing heavy metals (e.g., Pb, Hg, Cr, and Cd) were treated at 50, 600, and 900 °C to simulate their transformations caused by heat treatment prior to disposal or aging at a proper disposal site. The transformations were investigated by XRD, SEM, XANES, EXAFS, surface area measurements, pH static leaching tests, and extractions with oxalate and weak hydrochloric acid. It was found that at 600 and 900 °C the iron oxides were transformed to hematite, which had a greater thermo-dynamic stability but less surface area than the initial products. Heat treatment also caused some volatilization of heavy metals (most notably, Hg). Leaching with water at pH 9 (L/S 10, 24 h) and weak acid extraction showed that heat treatment caused a part of the metals bound in the oxides to be released, thus increasing metals leachability by 1–2 orders of magnitude depending on the metal. Pb and Cd were released in particularly significant concentrations, suggesting less incorporation into the iron oxides after heat-induced transformation. For Pb, this transformation of the chemical state of the bound metal was clearly supported by the X-ray absorption fine structure (XAFS) studies. A fraction of the bound Cr remained stable even after treatment at the highest temperature used in the study. It was concluded that the heat treatment of iron oxides may be advantageous to improve the thermodynamic stability of the product but that thermal treatment at both 600 and 900 °C significantly reduced the binding capacity for heavy metals.

Introduction

Iron (hydr)oxides are known to bind heavy metals through adsorption or coprecipitation (*1, 2*). Due to these mecha-nisms, iron oxides can control the distribution and concen-trations of heavy metals in aqueous systems and have been utilized in environmental technologies to remove metals from wastewater and liquid hazardous waste (*3*) and to pretreat air pollution control residues prior to landfilling (*4*).

If the heavy metal-containing iron oxides, in the form of sludge or solid residue from the treatment processes, are landfilled or used as fill material, it is important to consider the long-term stability of the metal binding. Freshly pre-cipitated iron oxides are amorphous or poorly crystallized. Their large surface area is advantageous for metal retention, but they are metastable and can over time undergo trans-formation into crystalline compounds such as hematite or goethite. The solubility of the latter crystalline phases is orders of magnitude lower than that of the amorphous solids, and the vulnerability of these compounds to microbial iron reduction is also considerably reduced (*5*). In this sense, the transformation from the amorphous to crystalline state may be advantageous for the long-term stability of the iron oxides, but the crystalline solids are likely to have diminished capacity to bind heavy metals.

The transformation of amorphous iron oxides into crystalline structures may proceed rapidly (within hours) in uncontaminated systems at high pH. It also may be extremely slow (months to several years) in strong salt matrixes, in which foreign ions (e.g., silicate) inhibit the formation of crystals (*6*). Heating accelerates the phase transition in iron oxides and can be used either as a part of treatment technology employed prior to the disposal of metal-bearing iron oxides or as experimental technique to study long-term changes anticipated to occur in a disposal site receiving these products. Previous studies of heat-induced transformation of sludges containing iron oxides have focused on the volume reduction (*7*). Changes of the metal binding capacity have primarily been studied in aqueous suspensions and at temperatures <100 °C (e.g., refs *8* and *9*). No information has been found regarding the influence of heat treatment at higher temperatures on the metal binding by these materials.

The purpose of this study was to quantify and explore the mechanisms associated with the changes of metal leaching from heavy metal-bearing iron oxides subjected to heating at 600 and 900 °C. Four samples (denoted henceforth as P0–P3) were prepared in the laboratory to represent various conditions and levels of metal enrichment. P0 contained no heavy metals and served as a reference for the iron oxide transformation in a silicium-containing salt matrix. P1 was precipitated in the presence of high concentrations of Pb, Cd, and Cr. P2 and P3 were precipitated in leachate from two types of air pollution control residues from municipal solid waste incinerators. Changes induced by the heat treatment were studied using X-ray diffraction (XRD), scanning electron microscopy (SEM), surface area determination (BET), dif-ferential thermal and thermogravimetric analyses (DTA/TGA). Metal leaching was characterized by aqueous and weak acid extractions. The crystalline structure and the binding of Pb were further examined using extended X-ray absorption fine structure (EXAFS) and X-ray absorption near edge structure (XANES) spectroscopies.

Materials and Methods

Preparation of Iron Oxides. $FeSO_4 \cdot 7H_2O$ was dissolved and oxidized by atmospheric oxygen in four different solutions stirred for 24 h. These solutions included two model systems and two leachates.

Model solutions P0 and P1 represented artificial leachates and were made by dissolving 109.92 g of $CaCl_2 \cdot 2H_2O$ (352

* Corresponding author telephone: +45 4525 1600; fax: +45 4593 2850; e-mail: mas@imt.dtu.dk.
† Technical University of Denmark.
‡ Department of Material Science and Engineering, University of Washington.
§ University of Illinois at Urbana–Champaign.
‖ Department of Civil and Environmental Engineering, University of Washington.

TABLE 1. Cation Content of the Four Model Products[a] at 50 °C (Based on Dry Mass)

composition	unit	product			
		P0	P1	P2	P3
Al	μg/g			194	128
Ba	μg/g			300	68
Ca	mg/g	167	167	163	107
Fe	mg/g	238	261	197	297
K	mg/g		59	30	43
Mg	mg/g			<0.2	<0.1
Mn	μg/g			340	489
Na	mg/g		0.4	7.2	19.2
As	μg/g			0.6	<0.7
Cd	μg/g		55	1.3	4.2
Co	μg/g			6.5	9.2
Cr	μg/g		397	7.0	17.7
Cu	μg/g			9.2	<2.2
Hg	μg/g			0.6	1.0
Mo	μg/g			14.3	58.2
Ni	μg/g			35.8	57.1
Pb	μg/g		7030	9648	8525
Zn	μg/g			144	197

[a] P0, product containing salts and no metals. P1, product containing salts and metals (Cd, Cr, and Pb). P2, product based on leachate from SD APC residue. P3, product based on leachate from FA APC residue.

mM) and 0.060 g of $Na_2SiO_3 \cdot 9H_2O$/L of Milli-Q water. P0 contained no heavy metals, while P1 was spiked with 3.18 g of $Pb(NO_3)_2$ (4.8 mM), 0.011 g of $Cd(NO_3)_2 \cdot 4H_2O$ (0.18 mM), and 0.30 g of $Cr(NO_3)_3 \cdot 9H_2O$ (0.38 mM). All used chemicals were of analytical grade.

Leachates P3 and P4 were produced using air pollution control (APC) residues received from two Danish municipal solid waste incinerator plants. These will be referred to as SD [semi-dry APC residue consisting of fly ash and dried Ca-$(OH)_2$ sprays from filter bags] and FA (fly ash from an electrostatic precipitator). Both leachates were produced by washing the APC residues for 24 h using a liquid to solid ratio (L/S) of 5 L/kg. Prior to the $FeSO_4$ addition, the leachates were filtered through filter paper with unspecified pore size.

After the addition of $FeSO_4 \cdot 7H_2O$, the iron concentrations in the suspensions were 179 mM for P0–P2 and 89 mM for P3. Throughout the entire oxidation period, the pH was kept constant at 10 by computer-controlled addition of 4 M KOH. After 24 h, sludges containing iron oxide were separated from the supernatant by vacuum filtering. The products were then dried at 50 °C. Table 1 contains the data regarding their initial chemical composition.

Heat Treatment. DTA and TGA were used to determine phase-transition temperatures of the products. DTA/TGA traces were obtained using a Netzsch thermal analysis instrument (model STA409). The 100–200-mg samples were analyzed in the temperature range of 25–1300 °C using a heating rate of 5 °C/min. The analyses were conducted in air.

Subsamples of the iron oxide products were treated thermally in a static uncontrolled atmosphere at 600 and at 900 °C. Samples were kept at 600 °C for 3 h or at 900 °C for 45 min. Treatment temperatures were reached within 15–20 min, and the samples were cooled to the room temperature within 30–60 min after treatment ended. All treatments were performed in a Lindberg box furnace. Heat treatment was performed using pure Al_2O_3 crucibles. Samples were lightly ground prior to analysis.

Characterization. The products were characterized before and after thermal treatment using the following methods and techniques:

Powder X-ray diffraction (XRD) was carried out using a Phillips PW 1830 X-ray diffractometer with filtered Cu–Kα radiation. Relevant peaks were identified using the Jade software.

The surface area was determined by the BET method using a surface area analyzer (Quantachrome Corp.). Helium was used as carrier gas, and N_2 was used as an adsorptive. To prevent structural changes, unheated samples were outgassed at a low temperature (50 °C).

Scanning electron micrographs (SEM) were obtained with a JEOL JSM 840A instrument. To avoid charging, all samples were sputter-coated with gold. The operating voltage was set at 10 or 15 kV. Micrographs were taken at a 2500× magnification.

The amorphous fraction of the iron oxides present in the samples was quantified by extraction (2 h in the dark) in 0.2 M ammonium oxalate at pH 3 (10).

To determine the total composition of the products before and after treatment, all samples were digested by autoclaving in 7 M HNO_3. Some uncertainty was introduced due to an incomplete dissolution of samples treated at 900 °C. Addition of concentrated HCl to these samples led to a more complete dissolution of the solids.

Metal Availability. Aqueous leaching tests were performed at a constant pH of 9. All tests were performed at a liquid-to-solid ratio (L/S) of 10 L/kg for 24 h. A computer controlled titrator kept the pH constant throughout the test period by adding either HNO_3 or KOH. Aqueous leachate samples were filtered using a 0.45-μm Millipore cellulose acetate filter and acidified with acetic acid prior to analysis.

The association of metals with the iron oxides was quantified by kinetic extractions of product P1 in 0.2 M HCl. In these experiments, 0.5 g of P1 was added to 150 mL of 0.2 M HCl [a modified method adopted from Kennedy et al. (11)]. The beaker was periodically centrifuged, and a 30-mL subsample was taken, while another 30 mL of 0.2 M HCl was added. Prior to measurements, the subsamples were filtered through a 0.45-μm polypropylene filter.

Synchrotron Measurements. EXAFS and XANES measurements were carried out at the UIUC/Lucent Technologies X16-C beamline of the National Synchrotron Light Source at Brookhaven National Laboratory (Upton, NY). The X-ray energy was varied from 200 eV below to 1000 eV above the absorption K-edge energy of Fe (7112 eV) and from 200 eV below to 500 eV above the absorption L_3-edge of Pb (13055 eV) using a Si(111) double-crystal monochromator. The Pb L_3-edge measurements were performed in the fluorescence mode using an argon-filled Stern-Heald ionization detector. A germanium filter (nine absorption lengths thick at the Pb L_3-edge energy) and Soller-type slits were used to minimize the fluorescence background. A 15-cm-long partially transparent gas ionization chamber was used to measure the incident X-ray intensity. It was filled with a mixture of 50% He/50% N_2 and 20% Ar/80% He for Fe K-edge and Pb L_3-edge measurements, respectively. Fe K-edge data were acquired in the transmission mode using a 30-cm-long ionization chamber filled with 20% Ar and 80% He to measure the transmitted beam intensity. To minimize harmonics in the Fe edge measurements, the monochromator crystals were detuned by ca. 25%. Detuning was not applied in Pb edge measurements. Data of up to 10 measurements were averaged for the same sample to improve the signal-to-noise ratio. Reference iron compounds (goethite and hematite) employed in the EXAFS measurements were prepared using methods described by Schwertmann and Cornell (10).

The EXAFS data were processed and analyzed using the UWXAFS software package (12). The smooth background functions were removed using the AUTOBK program (13), and the k^2-weighted (where k is photoelectron wavenumber) EXAFS functions $\chi(k)$ were obtained.
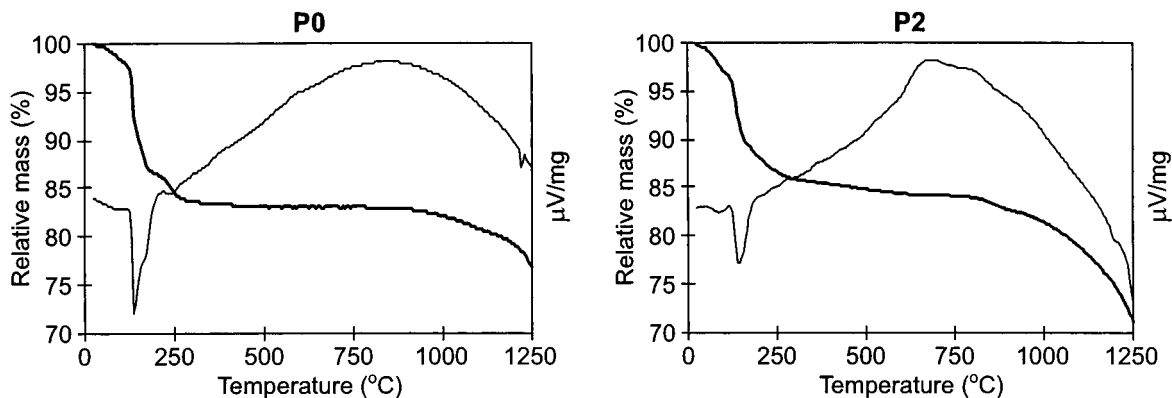
FIGURE 1. TGA/DTA diagrams for P0 and P2. TGA, bold lines; DTA, thin lines.

Metal Analysis. Metal concentrations were measured using one of the following techniques, depending on the metal and the concentration: inductively coupled plasma mass spectroscopy (ICP-MS), atomic emission spectroscopy (ICP-AES), atomic fluorescence spectroscopy (AFS), and atomic absorption spectroscopy (AAS) (flame and graphite oven atomization).

Results and Discussion

Effects of Heat Treatment on Iron Oxide Characteristics. As seen from the data presented in Table 1, Fe(II) oxidation and precipitation at high pH in the model solutions and leachates caused significant amounts of heavy metals to be trapped in the products. In contrast with the data for pure ferrihydrite (*1*), DTA analyses of these products did not reveal any distinct temperatures corresponding to a transformation of the crystalline structure (Figure 1). Only broad exothermic peaks were recorded in the temperature range of 700 and 900 °C. It is likely that the presence of foreign ions in the solids (notably, Si) caused the flattening and broadening of the corresponding peaks (*1*).

TGA (Figure 1) showed a distinct mass loss for all products at temperatures between 100 and 200 °C where water was released and again above ca. 1200 °C where the mass was lost due to vaporization. There was also a continuous but less distinct mass loss observed over the entire temperature range from 200 to 1200 °C for products P1–P3. This was likely to be caused by evaporation of material from the samples. Indeed, it is known that a part of the retained metals may be lost upon heating due to the vaporization as either pure metals or salts, mainly chlorides (*14, 15*). To reduce this risk, the treatment temperatures were chosen to obtain a change in the crystalline structure without loss of too much of the sample, particularly heavy metals present in the product. Moreover, the duration of the high-temperature treatment was adjusted to simulate the typical residence time in a sintering oven of an incinerator plant (45 min). For the lower temperature 600 °C, a treatment time of 3 h was chosen.

During heating, the appearance of the products changed, reaching almost purple color for products treated at 900 °C. According to Cornell and Schwertmann (*1*), this is consistent with a larger crystal size. This was confirmed by SEM data (Figure 2) that showed that some crystallization occurred in all products after drying at 50 °C. The crystalline structures detected by SEM may contain iron but were not identified by XRD analysis as such. It is also notable that after the thermal treatment the surfaces of the particles looked dusty, suggesting that some material was not integrated in the newly formed crystals but accumulated on the surface of the particles. In addition, the SEM micrographs clearly showed that partial melting or sintering of the particles took place during the 900 °C treatment. Due to the complexity of the products, a high number of peaks were observed on the

spectra. A full identification of the crystalline sample content was therefore not possible.

Consistent with the SEM evidence, surface area measurements showed a significant decrease of the surface area after thermal treatment (Table 2). The more complex products P2 and P3 showed larger areas at all temperatures than the two simpler products P0 and P1. The better crystallinity and stability of the products subjected to thermal treatment was confirmed by the presence of a smaller oxalate-extractable iron fraction (Table 3). The treatment at 900 °C resulted in products less dissolvable in the oxalate extract than those treated at 600 °C. This difference may be due to the larger crystal size and smaller accessible surface area as compared with those for products treated at 600 °C.

As seen from the TGA data, all four products lost considerable mass upon heating. The lost mass was primarily chemically bound water, but the evaporation of other elements also contributed. Using the data of total acid digestions and assuming that iron did not evaporate at the temperatures used, it was possible to determine the relative loss of metals (Table 4). The loss turned out to be minor for most metals analyzed in this work, except for Hg (for which the loss was significant at 600 °C and reached 76% in one sample at 900 °C) and Pb, 22–36% of which was lost at 900 °C. The uncertainty in the relative metal contents seen from Table 4 can be attributed to the low absolute metal contents and variations in the extent of digestion of the samples. Also, a minor fraction of the iron may have evaporated.

XRD analyses showed a lower background in the diffractograms of the thermally treated products. Again, this indicated that they contained less amorphous material than the untreated samples. The most significant crystalline phase present in the samples before treatment, gypsum, changed during heating to anhydrite due to the loss of water. EXAFS experiments showed that the crystalline structure around the iron ions in the unheated P1 was goethite-like. However, the goethite was never detected by XRD. This indicated poor long-range ordering of the iron oxides. The only iron-containing crystalline product identified by XRD in the treated samples was in all cases hematite. The presence of certain ions in amorphous iron (hydr)oxides has been proven to favor the formation of various crystalline solids (*1*). However, the presence of only hematite is consistent with the formation mechanism of this solid, which involves dehydration and recrystallization. The peaks in the XRD spectra of products treated at 900 °C were slightly sharper than those in the spectra of products treated at 600 °C. This indicated a higher degree of crystallization.

The local chemical environment around the Fe ions in the samples was studied by XAFS. The edge-step-normalized Fe K-edge X-ray absorption coefficients for the samples and two reference compounds (goethite and hematite) are shown in Figure 3. The spectra of the samples treated at 600 and 900
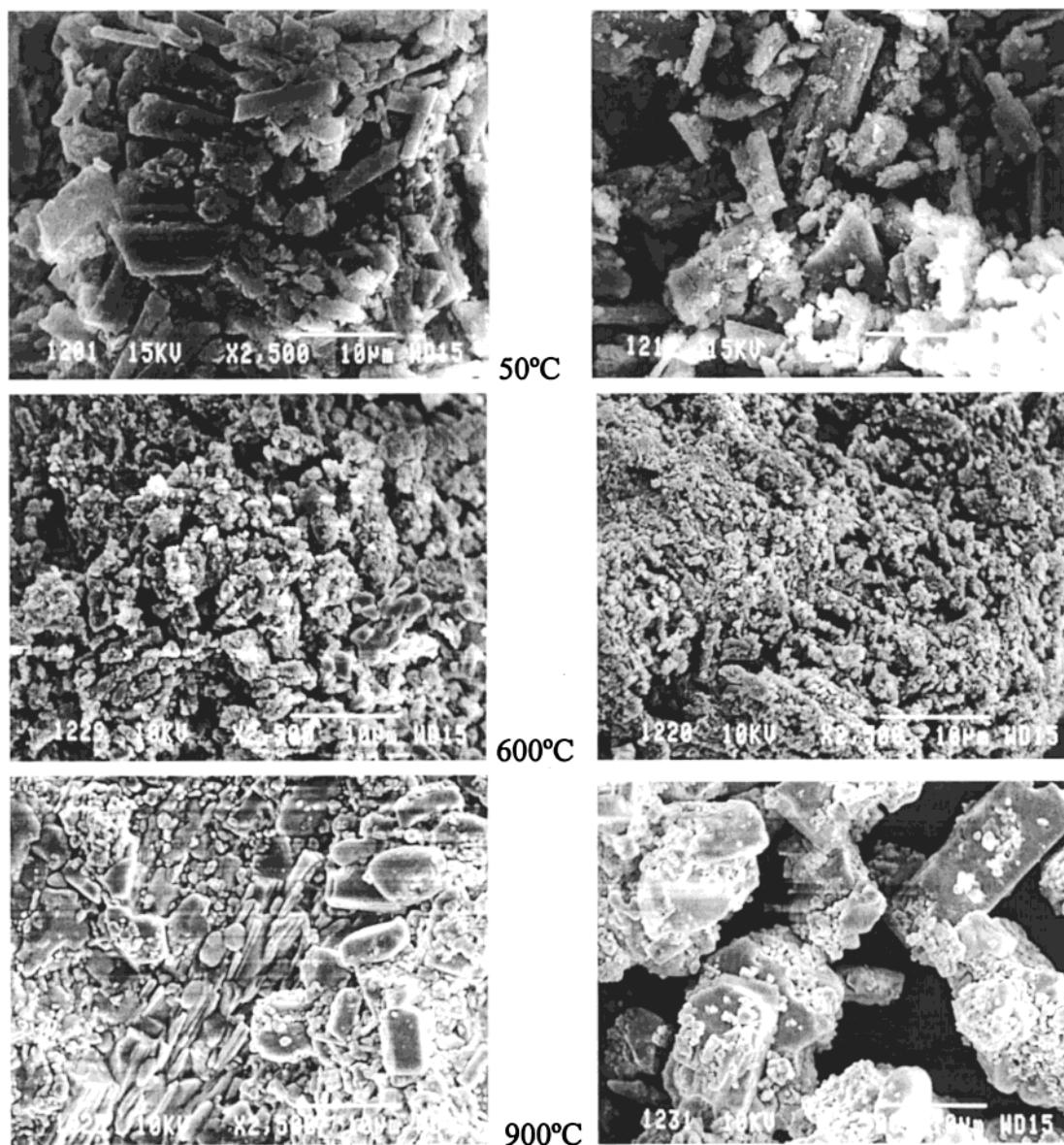
FIGURE 2. SEM pictures of P0 (left) and P2 (right) after treatment at 50, 600, and 900 °C.

TABLE 2. Surface Area (m²/g) (BET)

	50 °C	600 °C	900 °C
P0	19	7.1	0.3
P1	14	4.2	0.1
P2	23	13	0.3
P3	51	11	1.9

TABLE 3. Oxalate Extractable Iron Fraction (% of Total Content)

	50 °C	600 °C	900 °C
P0	39	2	0
P1	71	3	0
P2	61	7	0
P3	60	19	1

°C strongly resemble that of hematite, while the sample prepared at 50 °C exhibits distinctly different features in both the XANES (Figure 3, insert) and EXAFS regions. Its XANES spectrum and that of goethite have notable similarities in the 7122−7130 and 7170−7210 eV regions (Figure 3), while both of them differ dramatically from the spectra of all other samples. Thus, XANES indicates that the goethite structure approximates that of the local environment around the iron atoms in the 50 °C sample, albeit XRD did not detect a developed crystalline phase of goethite in the product. The conclusion regarding the similarities between the local structures around the Fe target in the 50 °C sample and in goethite and, on the other hand, between the 600 and 900 °C treated samples and hematite is in agreement with the data of Combes et al. (16).

The $k^2\chi(k)$ Fe K-edge data for all samples and reference compounds are shown in Figure 4. In the $k > 7$ Å^{-1} range, there is a striking difference in the amplitudes for the 50 °C sample and samples treated at higher temperatures. The origin of the decrease in the EXAFS signal intensity observed for goethite and the 50 °C sample at $k > 7$ Å^{-1} can be explained based on the structural data of the reference compounds. The Fe^{3+} ions in both goethite and hematite are octahedrally coordinated by oxygens, but the structures of the second nearest-neighbors (2NN) shell are different. In goethite (α-FeOOH), the 2NN shell includes 8 Fe atoms divided into three subgroups: 2 at 3.01 Å, 2 at 3.28 Å, and 4 at 3.46 Å (17). In hematite, the 2NN shell includes 13 Fe atoms divided into

TABLE 4. Relative Metal Content Determined on Acid Digestions and Based on the Assumption That Fe Acts as Conservative Element in the Solid Product

product	Me	Fe/Me[a]	50 °C	600 °C	900 °C
P1[b]	Fe	1	100	100	100
	Cd	10 500	100	126	98
	Cr	700	100	113	114
	Pb	150	100	113	59
P2[c]	Fe	1	100	100	100
	As	440 000	below detection limit		
	Cd	300 000	100	107	81
	Co	32 000	100	99	103
	Cr	26 000	100	102	115
	Cu	24 500	100	133	107
	Hg	1 145 000	100	74	24
	Mo	23 500	100	94	109
	Ni	5 800	100	97	88
	Pb	75	100	93	64
	Zn	1 600	100	104	92
P3[d]	Fe	1	100	100	100
	As	70 000	below detection limit		
	Cd	143 500	100	100	96
	Co	34 000	100	112	116
	Cr	15 500	100	114	110
	Cu	>155 000	below detection limit		
	Hg	1 100 000	100	85	56
	Mo	8 800	100	102	101
	Ni	5 500	100	105	94
	Pb	130	100	100	78
	Zn	1 800	100	113	108

[a] Fe/Me expresses the approximate iron content in the product relative to the metal content at 50 °C (mol/mol). [b] Salt and metal; only Cd, Cr, and Pb were added to this product. [c] Based on SD residue. [d] Based on FA residue.

four subgroups: 1 at 2.90 Å, 3 at 2.97 Å, 3 at 3.36 Å, and 6 at 3.71 Å (18). Since the backscattering amplitudes of the iron atoms at higher k numbers are larger than those of oxygen atoms, the increase in the amplitude of EXAFS oscillations for $k > 7$ Å^{-1} observed for samples treated at high temperatures correlates with the transition of the local structure around the iron ions from that of goethite to hematite.

The magnitudes of the Fourier-transformed $k^2\chi(k)$ data (not corrected for the phase shift functions) are shown in Figure 5. The Fourier transforms (FT) were performed in the k-range from 2 to 10 Å^{-1}, with the Hanning window margins of 2 Å^{-1}. The peaks located between 1 and 2 Å correspond to the Fe–O pair interactions and always have similar magnitudes, consistent with the octahedral coordination of the iron atoms by oxygens in all samples. The split of the 6 Fe–O distances into two subgroups containing 3 oxygens in each (at 1.95 and 2.09 Å in goethite and at 1.95 and 2.12 Å in hematite) is caused by the rhombohedral distortion of the FeO$_6$ octahedron in both model compounds. Given the similarity of the FeO$_6$ octahedron geometry in goethite and hematite, the stability of the FT magnitudes in this r range is not surprising.

The signal between 2 and 4 Å in Figure 5 is generated mainly by Fe–Fe pairs and reflects the relevant structural changes. The samples treated at 600 and 900 °C are evidently isostructural to hematite. The samples prepared at 50 °C and goethite have much lower FT magnitude in this distance range, which, as discussed, corresponds to the smaller number of the Fe atoms in the 2NN shell. However, the differences in the FT magnitudes for the 50 °C sample and goethite in the range of distances 2 and 4 Å should not be overlooked. Without a thorough structural analysis, it is impossible to separate the effects of bond length disorder (which is likely to differ for the amorphous 50 °C sample and polycrystalline goethite) from other structural effects, including the presence of nanocrystalline phases other than

goethite. For example, compounds similar to ferrihydrite (in which the radial distributions of the atoms in first several coordination shells around Fe are very similar to that in goethite) can also be formed in the 50 °C sample (19). Therefore, the range of distances in which the local environment around the Fe^{3+} ions in the 50 °C sample can be considered as isostructural to a goethite-like phase covers only the first and second nearest-neighbor shells.

In brief, the characterization of the iron oxides revealed that amorphous iron products with local quasi-goethite structure were transformed into hematite by thermal treatment at 600 and 900 °C. The higher was the temperature, the better was the ordering and the larger were the crystals formed. After treatment at 600 °C, the XRD peaks were relatively broad, and some iron remained extractable by ammonium oxalate, indicating an incomplete transformation or the presence of imperfections in the crystals especially prominent for the more complex products P2 and P3. Thus, the differences in metal and salt content of the four products resulted in noticeable differences in the structural ordering of the iron oxide products. After being heated to 900 °C, no iron was oxalate extractable from any of the products and the surface areas were significantly diminished, indicating that the amorphous iron oxide or hydroxide phase was no longer present in the two products. Hence, the inhibition of the phase transformation by contaminating ions (observed at 600 °C) was eliminated at 900 °C.

Effects of Heat Treatment on Metal Availability. The data on the leaching of heavy metals at pH 9 are shown in Table 5. At 50 °C, aqueous concentrations were less than 10 μ/L for all species. The total metal release corresponded to less than 0.1% of the solid content for most of the species except As, for which it was ca. 1%. For products P2 and P3 treated at 600 °C, metal release did not change dramatically except for a few specific metals, for which the leaching was increased (Zn for P2; Cr, Pb, and Zn for P3). For P1, which had a much higher content of Cd, Cr, and Pb, heating to 600 °C caused the leaching to increase substantially. The Cr leaching was 2% of the original content in the solid matrix. For Cd and Pb, leaching was very low (0.2% and 0.01%, respectively) but still much larger than for the 50 °C treated sample. However, the treatment at 900 °C caused the leachability of Cd and Pb from product P1 to increase by about a 1000-fold as compared with that for the 50 °C treated sample. 25% of the Cd and ca. 0.05% of Pb were released at a L/S ratio of 10 L/kg at pH 9. This suggested that these metals were expelled from the crystallized solids and formed much weaker bonds with the oxide carrier. Contrary to the trend for Pb and Cd, less Cr was leached from the 900 °C treated sample than from that treated at 600 °C (0.5 and 1.5% of the solid content, respectively). Similar patterns were observed for P2 and P3. Cd, Pb, and Zn leaching increased significantly following the 900 °C treatment, while Cr leaching decreased relative to the level observed at 600 °C. Leaching of As, Co, and Cu did not increase with the treatment temperature, while those for Mo and Ni increased somewhat. Leaching of Hg decreased following the high temperature exposure, but this is ascribed solely to the loss of Hg during the treatment (see Table 4).

The binding of Cd, Cr, and Pb was further examined by kinetic extractions of the heated and unheated P1 product. These experiments showed significant changes of the iron oxide stability and metal binding. As mentioned, the iron stability was significantly improved by the heat treatment, giving a very stable and practically insoluble products after exposures at 900 °C. However, the binding of all target metals (Pb, Cd, and Cr) deteriorated following the thermal process showing the lowest retention after heating to 900 °C (Table 6).

After treatment at 900 °C, lead and cadmium were readily extracted, meaning that they were expelled as the crystalline
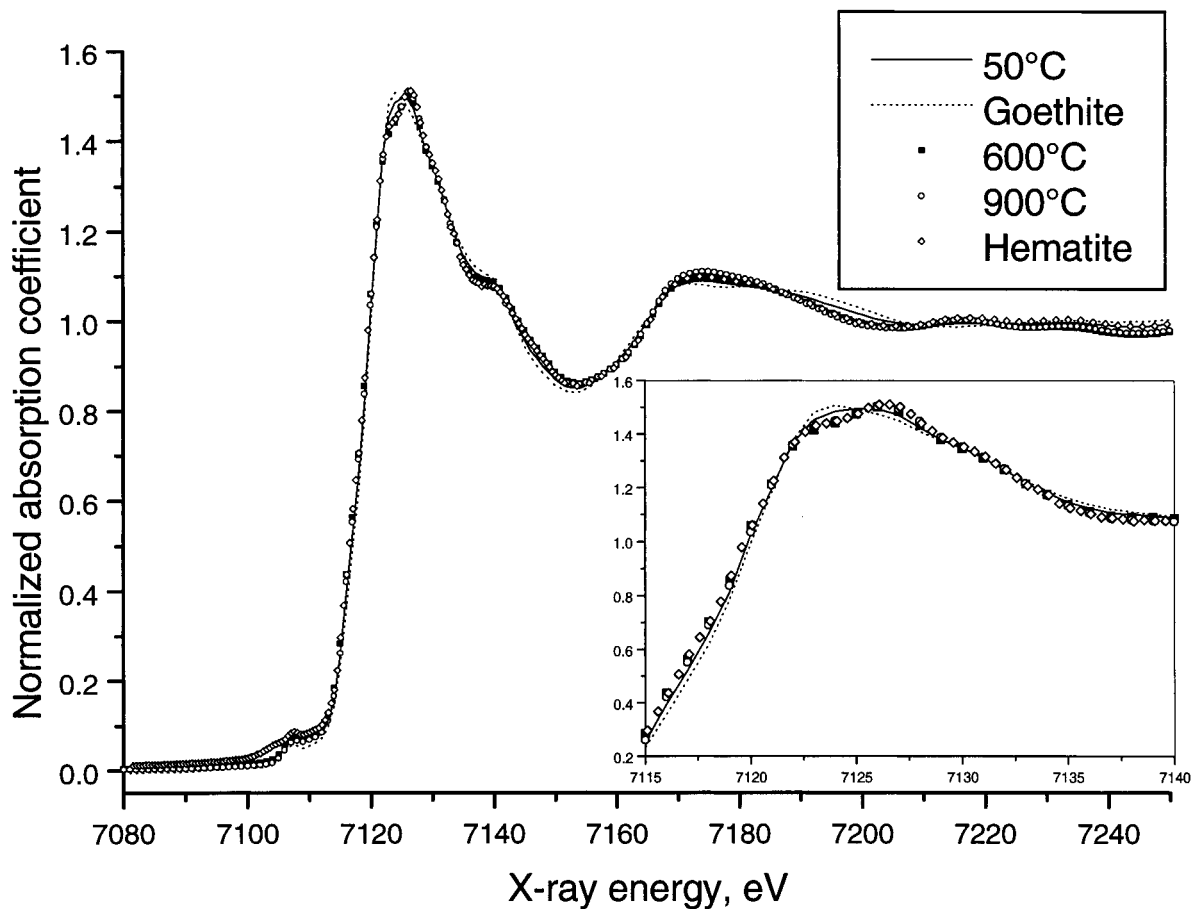
FIGURE 3. Edge-step normalized Fe K-edge absorption coefficients for the P1 iron product prepared with different heat treatments and for the two reference compounds, goethite and hematite.
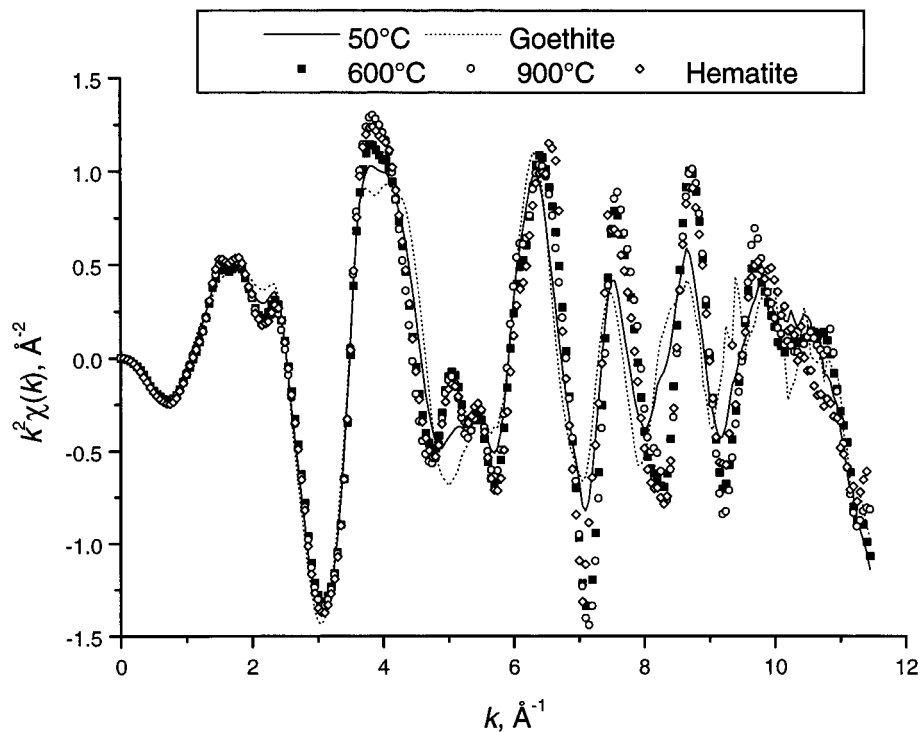
FIGURE 4. $k^2\chi(k)$ data for the P1 iron product prepared with different heat treatments and the reference compounds.

iron oxide structure formed. Lead showed an initially delayed release whereas cadmium was released practically instantly from the heat-treated products. Only a minor fraction of the trapped Pb was found in the leachate at pH 9. The great

difference seen in the release of cadmium and lead can be attributed to the fact that Pb^{2+} is known to sorb on iron oxide surfaces much more strongly than Cd^{2+} (20). Chromium, on the other hand, showed an initial high release following
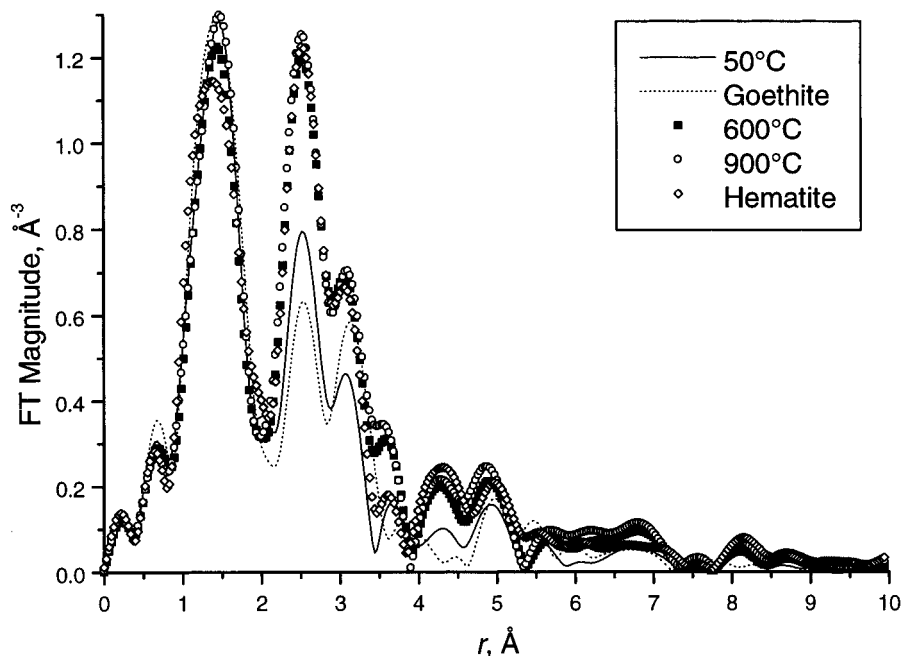
FIGURE 5. Magnitudes of the Fourier-transformed $k^2\chi(k)$ data for the P1 iron product prepared with different heat treatments and the reference compounds.

TABLE 5. Leaching of Metals (Mass of Metal/Dry Product Mass)[a]

product	metal (μg/kg)	50 °C	600 °C	900 °C
P1[b]	Cd	15	109	14 000
	Cr	3.5	5 685	214
	Pb	1.4	573	1 670
P2[c]	As	48	10	16
	Cd	<1.0	2.1	351
	Co	2.4	5.5	4.2
	Cr	3.3	32	5.2
	Cu	<20	<20	<20
	Hg	1.6	0.6	0.4
	Mo	47	17	193
	Ni	<10	<10	31
	Pb	39	27	6 180
	Zn	<40	257	3 410
P3[d]	As	32	59	119
	Cd	<1.0	<1.0	80
	Co	3.3	2.4	2.3
	Cr	11.3	564	306
	Cu	<20	<20	<20
	Hg	0.7	<0.2	<0.2
	Mo	27	82	700
	Ni	<10	<10	23
	Pb	8	165	1 700
	Zn	63	5 550	274

[a] At pH 9, L/S 10 L/kg, 24 h. [b] Salt and metal; only Cd, Cr, and Pb were added to this product. [c] Based on SD residue. [d] Based on FA residue.

TABLE 6. Metal (% of Total Content) Extracted from P1 with 0.2 M HCl

element	time (h)	50 °C	600 °C	900 °C
Fe	0.25	3	0	0.0
	0.5	4	1	0.1
	0.75	5	1	0.1
	1	5	1	0.1
	4	11	7	0.1
	48	25	13	0.2
	216	35	27	0.8
	1536	58	64	6.3
Cd	0.25	12	38	92
	0.5	14	48	88
	0.75	12	52	91
	1	12	54	91
	4	16	67	90
	48	26	73	91
	216	30	76	91
	1536	45	88	92
Cr	0.25	9	14	43
	0.5	12	19	46
	0.75	15	23	49
	1	17	27	51
	4	28	45	54
	48	41	56	59
	216	48	60	60
	1536	60	82	62
Pb	0.25	31	34	72
	0.5	33	40	72
	0.75	34	41	72
	1	36	51	87
	4	43	74	88
	48	69	82	102
	216	73	85	102
	1536	77	93	105

heating to 900 °C, but after extraction of 60% of the total content the dissolution of Cr stopped, indicating that the remaining 40% were very stable. This could indicate that a fraction of the Cr remains integrated in the dense crystalline structure of iron oxides. The amount of chromium released from the samples treated at 900 °C was lower as compared with that at 600 °C. The extracted Cr fraction in the 600 °C sample exceeded that of the 900 °C sample after approximately 500 h of extraction.

Thus, heating to 600 °C was not advantageous for any purpose. The iron oxide stability was not improved, although a more crystalline structure was formed according to the mineralogical analyses. The release of trace metals increased substantially as compared to the release from the unheated product. Therefore, it is concluded that heating does not provide better binding of trace metals in the crystalline structures. A minor advantage was observed only for Cr.

X-ray absorption analyses on sample P1 prior to and after the thermal treatment provided more information regarding the changes in binding of Pb to the iron oxide surface. For
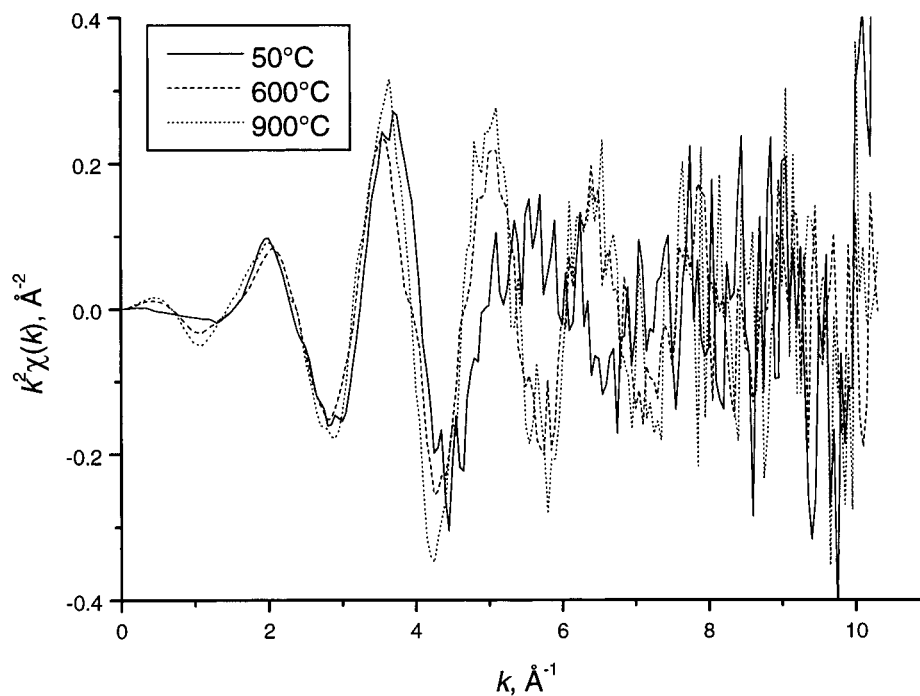
FIGURE 6. k^2-weighted $\chi(k)$ Pb L_3-edge data for the P1 iron product prepared with different heat treatments.
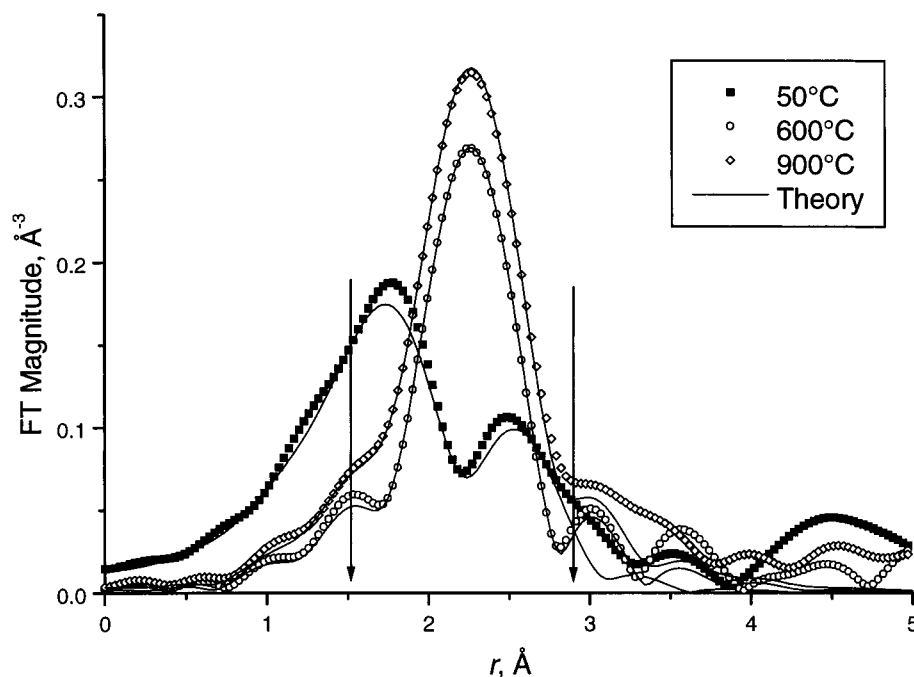
FIGURE 7. Magnitudes of the Fourier-transformed Pb L_3-edge data (symbols) for the P1 iron product prepared with different heat treatments and theoretical fits (solid), performed between 3 and 9 Å^{-1}. The arrows indicate the fitting range.

Cd and Cr, similar information could not be obtained since their concentrations in the samples were too low. The Pb L_3-edge k^2-weighted $\chi(k)$ data and the magnitudes of their Fourier transforms (performed between 3 and 9 Å^{-1}) for all the three iron products are shown in Figures 6 and 7, respectively. It is obvious that dramatic changes occurred in the local structure around the Pb atoms in the 50 °C sample and the other two samples studied. The data of the 600 and 900 °C samples have a single peak between 1.8 and 2.8 Å, while in the spectrum of the 50 °C sample there are two peaks located between 1.5 and 2.2 Å and between 2.2 and 3 Å, respectively (Figure 7).

To explain the second peak in the 50 °C sample spectrum, it is relevant to consider a model in which a significant fraction of Pb^{2+} ions is incorporated in the quasi-goethite structure discussed in the preceding section. This model presumes the presence of iron atoms in the 2NN shell. As shown for the 2NN Fe–Fe interactions in the Fe K-edge measurement (Figure 5), the 2NN Pb–Fe pair interactions would noticeably contribute to the EXAFS signal and manifest themselves as a second peak in the FT magnitudes.

Quantitative exploration of the EXAFS data for lead is challenging due to a high variability of its coordination number (e.g., refs 21 and 22). These cited papers contain a compilation showing a very high range of both the Pb–O distances and coordination numbers reported for reference compounds. Model-specific analysis, which requires a priori assumptions regarding the geometry of the atomic arrange-

TABLE 7. Compilation of EXAFS Fitting Results for Lead

sample	Pb coordination no.	Pb–O distances (Å)	Pb–O bond disorder (Å²)	no. of Fe atoms in 2NN shell	Pb–Fe distances (Å)
cerussite (ref)	8.5 ± 2.9	2.61 ± 0.03	0.020 ± 0.007	na[a]	na
product 1 at 50 °C	4.7 ± 0.9	2.38 ± 0.02	0.022 ± 0.004	1.9 ± 1.2	3.17 ± 0.02
product 1 at 600 °C	2.4 ± 0.1	2.70 ± 0.01	0.0030 ± 0.0004	na	na
product 1 at 900 °C	4.7 ± 0.2	2.73 ± 0.01	0.0109 ± 0.0007	na	na

[a] na, not applicable.

ment for the nearest-neighbor oxygens, is inapplicable since too many adjustable parameters relative to the number of independent data points must be used. However, it is possible to quantify the average Pb–O distances and the total number of O neighbors around the Pb atoms, provided that the spread in the individual Pb–O distances is not too large.

We tested the fitting procedure for cerussite ($PbCO_3$). The data analysis was performed using FEFF7 theory (*23*) and the computer code FEFFIT (*12*). The latter code performs nonlinear least-squares fits and estimates uncertainties in the results. The FEFF7 theoretical estimate of single Pb–O contributions was calculated using the known crystalline structure of cerussite and then fit to its EXAFS spectrum processed in the same conditions as those used for the iron oxide products. The number of O atoms, average Pb–O bond length and its disorder (σ^2) were varied in the fit. The results are compiled in Table 7. The best-fit result for the coordination number (8.5 ± 2.9) and the average distance (2.61 ± 0.03 Å) for cerussite were in good agreement with the available structural data (*24*). The total number of O atoms was 9, and the Pb–O distances were from 2.62 to 2.77 Å.

After the fitting procedure was successfully tested for the reference compound, we applied the same model to fit the Pb L_3-edge EXAFS data in the iron products. The best-fit results for the iron oxide products treated at 600 and 900 °C (see Table 7 and Figure 7) are as follows. The average Pb–O coordination numbers are 2.4 and 4.7, their distances are 2.70 and 2.73 Å, and the disorders in these distances are 0.0030 and 0.0109 Å², respectively. It is notable that the lead coordination number and the disorder in Pb–O bond in the 900 °C sample increase relative to that in the 600 °C sample. Since the force constant of the Pb–O pair interaction is inversely proportional to σ^2, the increased disorder mean that the Pb–O bond strength is weakened in the high-temperature sample. The nature of the low coordination number obtained for the iron oxide product treated at 600 °C cannot be explained at present. Although similarly low coordination numbers have been reported in the literature for selected model compounds [e.g., β-PbO and $PbSiO_3$ (*21*)] and for adsorbed lead species (*22*), the exact scenario of transformations of the Pb environment associated with the increase of the treatment temperature from 600 to 900 °C remains uncertain.

The structural state of the lead in both these specimens is very different from that in the 50 °C sample, as anticipated from the difference between the raw data (Figure 7). In the latter sample, the average coordination number was 4.7, the Pb–O distances were shorter (2.38 Å), and the disorder was 0.022 Å². To explain the second peak in the 50 °C sample spectrum (Figure 7), it is relevant to consider the incorporation of a significant fraction of Pb^{2+} ions into the iron(III) hydr(oxide), whose structure can be modeled by that of goethite [or other structurally similar iron(III) (hydr)oxides]. Since this presumes the presence of Fe atoms in the second coordination shell, 2NN Pb–Fe interactions were accordingly included in the model employed to fit the data in the second peak region. The number of Fe atoms corresponding to this feature was determined to be 1.9 ± 1.2, while the Pb–Fe distances were 3.17 ± 0.02 Å.

These results of the EXAFS analysis of Pb L_3-edge data indicate that Pb atoms partially substitute the iron centers in the iron (hydr)oxide matrix and appear to be integrated in the bulk of the 50 °C sample. This type of lead bonding is eliminated by high temperature treatment, which causes the retained lead to segregate from the oxide matrix and eventually weakens the Pb–O bond strength (notably, in the 900 °C sample). This conclusion supports the extraction data that showed a dramatic increase of lead release associated with thermal treatment of the samples.

Environmental and Technological Implications. The concept of heat treatment of iron oxide-based sludges containing heavy metals was examined with respect to changes of the long-term stability and metal binding. Analyses showed the heat-induced transformation of amorphous iron (hydr)oxides to crystalline hematite caused most of the retained heavy metals to accumulate on the surface of the particles. Consequently, the leachate concentrations of these metals increased. Following this transformation, surface adsorption played a major role in controlling the leachate composition, since most contaminating cations were accumulated on the surface and not in the iron (hydr)oxide bulk. The best binding of heavy metals and thereby their slowest release was observed for the unheated products. Hence, although the thermodynamic stability of amorphous iron (hydr)oxides is significantly lower than that of crystalline iron oxides, a thermally forced transformation to the crystalline form is not recommended. Natural aging of the sludge products may result in similar transformations of the amorphous iron (hydr)oxides, but the presence of contaminating ions is likely to significantly retard this process. Since the expected transformation is not artificially accelerated, the crystalline end products will not necessarily resemble closely packed hematite. Another frequently found and stable iron oxide (goethite) may be formed instead. Goethite has been proven able to bind significant amounts of various metal cations (e.g., ref *25*) and can be expected to retain a higher content of foreign cations in a naturally aged iron (hydr)-oxide sludge.

Acknowledgments

Literature Cited

(1) Cornell, R. M.; Schwertmann, U. *The Iron Oxides*; VCH: Weinheim, 1996.

(2) Stumm, W.; Morgan, J. J. *Aquatic Chemistry*; John Wiley and Sons: New York, 1996.

(3) Benjamin, M. M.; Sletten, R. S.; Bailey, R. P.; Benett, T. *Water Res.* **1996**, *30*, 2609.

(4) Lundtorp. K.; Jensen, D. L.; Sørensen, M. A.; Mogensen, E. P. B.; Christensen, T. H. *Waste Manage. Res.*, submitted for publication.

(5) Postma, D.; Jakobsen, R. *Geochim. Cosmochim. Acta* **1996**, *60*, 3169.

(6) Cornell, R. M.; Giovanoli, R.; Schindler, P. W. *Clays Clay Miner.* **1987**, *35*, 21.

(7) Baltpurvins, K. A.; Burns, R. C.; Lawrance, G. A.; Stuart, A. *Environ. Sci. Technol.* **1996**, *30*, 939.

(8) Martinez, C. E.; Mcbride, M. B. *Environ. Sci. Technol.* **1998**, *32*, 743.

(9) Martinez, C. E.; Mcbride, M. B. *Clays Clay Miner.* **1999**, *46*, 537.

(10) Schwertmann, U.; Cornell, R. M. *Iron Oxides in the Laboratory; Preparation and Characterization*; VCH: New York, 1991.

(11) Kennedy, L. G.; Everett, J. W.; Ware, K. J.; Parsons, R.; Green, V. *Bioremed. J.* **1998**, *2*, 259.

(12) Stern, E. A.; Newville, M.; Ravel, B.; Yacoby, Y.; Haskel, D. *Physica B* **1995**, *208–209*, 117.

(13) Newville, M.; Livins, P.; Yacoby, Y.; Rehr, J. J.; Stern, E. A. *Phys. Rev. B* **1993**, *47*, 14126.

(14) Jakob, A.; Stucki, S.; Kuhn, P. *Environ. Sci. Technol.* **1995**, *29*, 2429.

(15) Chan, C.; Jia, C. Q.; Graydon, J. W.; Kirk, D. W. *J. Hazard. Mater.* **1996**, *50*, 1.

(16) Combes, J.-M.; Manceau, A.; Calas, G. *Geochim. Cosmochim. Acta* **1990**, *54*, 1083.

(17) Szytila, A.; Burewicz, A.; Dimitrijewic, Z.; Krasnicki, S.; Rzany, H.; Todorovic, J.; Wanic, A.; Wolski, W. *Physica Status Solidi* **1968**, *26*, 429.

(18) Blake, R. L.; Hessevick, R. E.; Zoltai, T.; Finger, L. W. *Am. Mineral.* **1966**, *51*, 123.

(19) Manceau, A.; Drits, V. A. *Clay Miner.* **1993**, *28*, 165.

(20) Schultz, M. F.; Benjamin, M. M.; Ferguson, J. F. *Environ. Sci. Technol.* **1987**, *21*, 863.

(21) Manceau, A.; Boisset, M.-C.; Sarret, G.; Hazemann, J.-L.; Mench, M.; Cambier, P.; Prost, R. *Environ. Sci. Technol.* **1996**, *30*, 1540.

(22) Strawn, D. G.; Scheidegger; A. M.; Sparks, D. L. *Environ. Sci. Technol.* **1998**, *32*, 2596.

(23) Zabinsky, S. I.; Rehr, J. J.; Ankudinov, A. L.; Albers, R. C.; Eller, M. J. *Phys. Rev. B* **1995**, *52*, 2995.

(24) Sahl, K. *Z. Kristallographie* **1974**, *139*, 215.

(25) Gerth, J. *Geochim. Cosmochim. Acta* **1990**, *54*, 363.